International Research Journal of Engineering and Technology (IRJET) e-ISSN: 2395-0056
Volume: 11 Issue: 05 | May 2024 www.irjet.net p-ISSN: 2395-0072

Graphene-dye nanocomposite for advanced solar cell applications: Combined experimental and theoretical study

Prosenjit Choudhury[1] Md. Nur Alam[2], Ankana Karmakar[3], Amitava Mandal[4], Md.Rabiul Islam[1*]

[1]Department of Physics, Dr. Meghnad Saha College, Itahar-733128, India,
[2]Department of Physics, Raiganj University, Raiganj-733134, India
[3,4]Department of Chemistry, Raiganj University, Raiganj-733134, India
**Corresponding Author Name: Dr. Md.Rabiul Islam*

Abstract

In this work, a composite system comprised of Methyl Orange dye (MO) and reduced graphene oxide(rGO) system was designed and synthesized. Graphene has been synthesized from graphite flakes by oxidation using improved method. Reduced graphene oxide (rGO) was obtained via simple reduction treatment of GO (graphene oxide) powder. rGO was utilized as non-fullerene acceptor material owing to its lower value of LUMO energy level. Furthermore, its exceptional electron accepting also supported by density functional theory-based calculation. An organic solar cell is fabricated using rGO together with Methyl Orange as standard donor material in ambient atmosphere. Photo response in photoconduction mode have been observed which increases with bias voltage. Investigation of dark I-V characteristics reveals trap charge limited conduction processes within the device. This sort of stable organic material can simply be utilized in fabricating organic solar cell and hence it can be used as one of the best alternatives as non-fullerene acceptor materials.

Keywords

Organic solar cell, graphene-based organic nanomaterials, non-fullerene acceptor, dye-based acceptor at ambient temperature, DSSC, DFT

1. Introduction

Need of the day is environment-friendly renewable energy production because advancement of civilization demands higher energy production. Conventional energy sources are comprised of fossil fuels and nuclear energy sources. Burning of fossil fuels produces green-house gases which in turn are responsible for global climate warming and related catastrophic events like extreme weather conditions, melting of ice in polar region etc. In addition, the resources of fossil fuels are limited. Nuclear reactors on the other hand possess the threat of radioactive- wastages. To help avoid these potential threats from conventional energy resources solar cell is the best alternative. Though inorganic solar cells are greatly being used now-a-days, but these devices have the disadvantage of high processing cost. Organic photo-voltaic (OPV) emerged in 80's as a possible replacement. Since the inception, organic solar cells grabbed the eye of scientific community. The primary benefits associated with using organic solar cells (OSC) are simple processing techniques, mechanical flexibility and large stock of materials that can be tailored to desired level of band gaps (here difference between LUMO and HOMO level) [1-9]. At present, the OPV technology is at 3rd generation. Now a days the most recent third generation solar cells include perovskite solar cells, polymer based solar cells, dye sensitized solar cells. Among these, the dye sensitized solar cells (DSSCs) has attracted much attention in worldwide due to its simple processing techniques, flexibility and low cost [10]. However, the power conversion efficiency (PCE) and long-term operational stability of DSSCs are not up to the mark for practical applications, in comparison to traditional silicon-based solar cells. Consequently, tremendous research efforts are going on to realize high performance and sustainable devices by introducing novel materials and new synthesis techniques. As a consequence of their remarkable optoelectronic, mechanical, thermal, and chemical properties, novel materials, particularly carbon-based ones like graphene and its derivatives, have the greatest possibility to replace or alter the traditional materials that are often used in the creation of the various DSSC components. Additionally, the recent use of graphene-based materials as photoanodes—transparent conducting anodes, semiconducting layers and dye-sensitizers, electrolytes and counter cathodes in DSSCs [11]. Graphene derivatives finds its application mostly as anodes [12-13] and Cathodes [14-17]. However, the utilization is somehow limited. Graphene may also be utilized as acceptor material [18-20]. For the dye component aromatic azo compound like Methyl

orange (MO) is the attractive option due to their easy synthesis, high environmental stability and their tunability issues. Azo dyes are well-known photoactive materials owing to their good chemical stability, good optical switching property and high solution process ability [21]. In this context, we have designed, synthesized and characterized a dye based organic solar cell with Methyl Orange and reduced Graphene Oxide blend, as a new photoactive material. It It possesses a lower energetic lowest unoccupied molecular orbital (LUMO) level, stronger electron accepting ability noteworthy solubility in distill water. The photovoltaic cell comprises of a thin layer of blends of organic dye Methyl Orange and graphene in form of dust (rGO), which serves as the optical active material. To comprehend the performance of the device, the dark I-V characteristics is examined in laboratory. Sampietro et al. illucidates the current voltage characteristics of organic solar cells. They demonstrated the existence of three distinct regimes within the current voltage dependence [22]. It is well known that trap centers arising from different defects due to structural disarray play a noteworthy role in the current conduction mechanism. These generated traps sates will invite energy levels in between the HOMO-LUMO energy levels providing ease of transport. With increased energy below the LUMO, the dispersion of these trap levels may shrink exponentially. The operation of the device depends heavily on the charging and discharging of these trap levels. The charge transport and semiconducting properties of organic materials are quite different from their traditional inorganic equivalent due to the polymer's crystalline-amorphous nature and the delocalization of the electric field along the π-conjugated segments of the polymer backbone. The I-V characteristics demonstrate that, like other organic material-based devices, the same device is governed by a trap-assisted model. The outcomes have been successfully explained by the assumption that there is an exponential trap distribution [23-24]. Additionally, DFT calculations have been carried out to understand the Energy diagram of the system, UV simulation of Methyl Orange dye, UV data excitation energy analysis, HOMO -LUMO of the rGO-Methyl Orange composite.

2. Experimental Section

2.1 Materials and methods:

The chemicals used to prepare the dye based rGO nanocomposites are (i) `PVA procured from NICE CHEMICALS (P) LTD, (ii) Methyl Orange dye procured from LOBA CHEMIE PVT LTD and (iii) Graphite Fine Powder procured from LOBA CHEMIE PVT LTD. All materials are used as received without further purification.

2.2 Synthetic procedure of preparation of Graphene Oxide:

Graphite flakes were oxidized using the recent method. 9:1 mixture of concentrated H_2SO_4/H_3PO_4 (360:40 mL) was poured into a mixture of graphite flakes (3.0 g, 1 wtequiv) and $KMnO_4$ (18.0 g), and exposed to 35-40 °C. The reaction was then heated to 50 °C and stirred for 12 h. The reaction mixture was then cooled to normal room temperature and kept on ice (400 mL) with 30% H_2O_2 (3 mL). After that centrifugation was done (4000 rpm for 4 h), and decantation was carried out. The remaining solid material was then washed in succession with 200 mL of water, 200 mL of 30% HCl, and 200 mL of ethanol for each wash, the mixture was sifted then filtered and the filtrate was centrifuged (4000 rpm for 4 h) and followed by decantation was done. The solid obtained by the filtration process was dried in vacuum overnight at room temperature, obtaining 5.8 g of product [25].

2.3 Synthesis of reduced graphene oxide:

After achieving the above steps, reduced graphene oxide (rGO) was obtained via simple reduction treatment of GO (graphene oxide) powder. The GO powder was annealed at various temperatures (200, 300 and 400 ^oC) in oven. During annealing process Graphene Oxide changed to dark powder as rGO material. The alteration is caused by the decrease of oxygenated functional group on GO sheets [26]

2.4 Computational Methods:

In this study, density functional theory (DFT) was employed using the Gaussian 16 program to perform all theoretical calculations [27]. The ground state geometry optimizations of Methyl Orange (MO), Reduced Graphene Oxide(rGO), and the MO-rGO composite system were conducted at the B3LYP/6-31+G(d) level of theory. The hybrid functional B3LYP offers reliable and precise energy values of non-covalently bonded interactions for hydrogen bonded and π–π stacked systems. The Polarizable Continuum Model (PCM) was applied to introduce solvent effects (water) during the ground state optimization [28]. TD-DFT calculations are performed ata the same level of theory. Vibration frequency analysis was performed at the same

level of theory (no imaginary frequency) and subsequently no imaginary frequency clearly indicates that the geometries corresponds to the minima at the potential energy surface. The visualization of various weak interactions such as H-bonding, van der Waals interactions, and steric interactions was achieved by reduced density gradient (RDG) using the Multiwfn 3.7 suite [29]. The nature of electronic transitions in terms of involved molecular orbitals (MOs) are interpreted by using Gaussum3.0[30-32]. In order to assess the degree of charge-transfer interactions within the Methyl Orange- reduced graphene oxide complex system in a water medium, molecular electrostatic potential (MESP) maps were created using the same level of theory. The adsorption energies (ΔE_{ads})of the complex system were determined using the following equation.

$\Delta E_{ads} = E_{rGO-MO} - E_{rGO} - E_{MO}$

Where, $E_{rGO-MO}, E_{rGO}, E_{MO}$ are the total energy of the geometry optimized complex system, reduced graphene oxide and the methyl orange dye respectively.

2.5 Device fabrication:

Dey et al. fabricated a photovoltaic cell by sandwiching an organic photoactive material between two electrodes [33]. We have followed the similar technique for device fabrication. In the research described here, the photovoltaic cell is made up of a thin layer of blends of organic dye Methyl Orange, and graphene in form of dust (rGO), which serves as the optical active material. This mixture serves as the active material in the cell in the form of a thin film. One transparent glass plate coated Indium-Tin-Oxide (ITO) serves as the contact electrode, and the other contact electrode is made of aluminum. Methyl Orange dye is mixed with polyvinyl alcohol (PVA). After that PVA solution is done by mixing 1 gm of PVA with 20ml of distilled water in a test tube, followed by warming and stirring gently. 1 mg of graphene is mixed with this solution. PVA is utilized here as an inert transparent binder to form stable film of the dye. The mixture is stirred and heated to a temperature of 80◦C for 2h. The viscous solution is sandwiched between transparent ITO-coated glass and aluminum plate. Both the ITO coated glass plate and aluminum plate were cleaned in alcohol solution and dried for approx 1h before use. The two electrical leads are taken out of the two ends of the electrodes. The entire cell is vacuum dried for about12 hour around 60◦C before the final measurement.

2.6 Experimental setup:

As seen in Figure 1, the PV cell is biased using a d.c. source (making the ITO contact the anode and the aluminum plate cathode). A Mastech MAS830L multimeter is used to measure the voltage across a 33 KΩ resistance to determine the current flowing through the device.

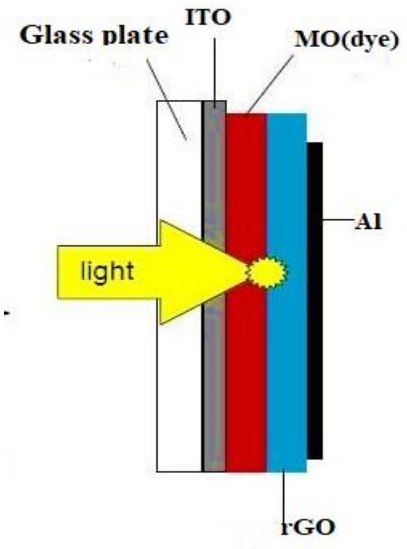

Fig- 1. Structure of the photo voltaic cell. A thin film of blend made of Methyl Orange, complexed with PVA and dust of graphene, is sandwiched between one ITO coated glass plate and aluminum plate. (The dc source and external resistance is not shown in this figure)

In order to obtain the dark, I-V characteristics, the bias voltage is increased from 0 volt to 5 volts. The step of increment is 0.2-volt up to 3 volt and the same is 0.5 volt after that. The current is found in microampere range. This range of output current is quite beneficial for solar cell applications because it determines the amount of power that can be generated from the device. The higher the current higher will be the power as well as the efficiency of the device. However, the current is seen to be depending on various factors such as material thickness and morphology. After applying each bias voltage, it is seen that the current takes some time (a couple of minutes) to attain its steady-state value. For both forward and reverse bias, the I-V properties are roughly symmetric about the origin. For measurement of photocurrent, a tungsten lamp of 100 watt was illuminated and light was allowed to enter the cell through ITO coated glass plate. The bias voltage is increased to 0.5 to 3 volts with a step of 0.5 volt. At each bias voltage the variation of photocurrent with time is recorded.

3. Results and discussion

3.1 Experimental Findings

3.1.1 Dark I-V characteristics:

The data of applied bias voltage and corresponding measured currents are plotted and the corresponding log V-log I are also obtained by using OriginPro software (shown in figure 2). The log V-log I Plot shown in depicts a transition point at a bias voltage of roughly 1.2 volt, indicating a shift in the conduction mechanism at this bias voltage. By utilizing [2] the relation $E_g = eV_{on}$, we calculate E_g= 1.2 eV (whereas, theoretically it was found to be1.03 eV)

The I– V relation shown in the figure below can be written as,

$$I \propto V^{0.487} \text{ for } V<1.2V$$

$$\propto V^{1.53} \text{ for } 1.2V<V<5V$$

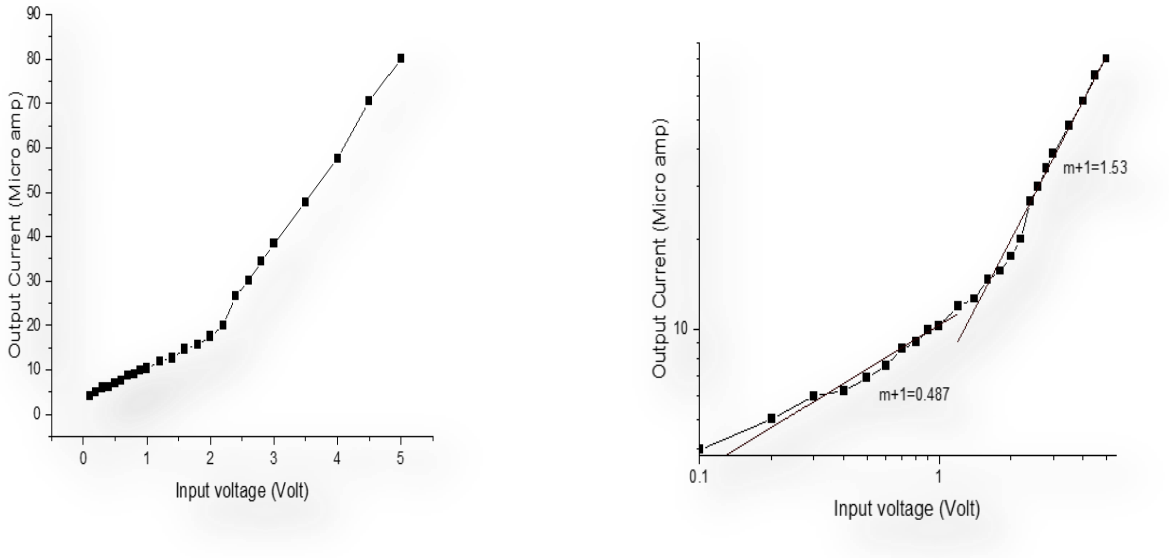

Fig-2. Dark I-V characteristics of the photovoltaic cell(left) and its log- log plot(right)

To analyze the dark,I-V characteristics, the following model for conduction mechanism may be approximated. The lowest unoccupied molecular orbital (LUMO) states, which are like conduction band, and the highest occupied molecular orbital (HOMO) states, which are just like the top of the valence band, are possible places for carriers to be transported during conduction within the device, As documented in the literature [18-20]. A model based on trap charges that are states having energies in between HOMO and LUMO level is taken into consideration to explain the modification of the conduction process.

One-dimensional single (double) carrier drift current and Poisson equations (for electrons, holes, or both) serve as the starting equations,

$$J = ne\mu E \qquad (1)$$

$$\nabla^2 V = -(n + n_t)e/\varepsilon \qquad (2)$$

Where J is the current density, μ is the carrier mobility, E is the electric field strength, n and n_t are the free and trapped charge concentrations respectively, e is the unit charge and ϵ is equal to $\epsilon_0 k$, with ϵ_0 being the permittivity of vacuum and k the relative dielectric constant. When traps have an exponential energy distribution, the trap charge concentration (n_t) is given by,

$$n_t = H_n \exp(F_n/k_B T_t) \quad (3)$$

Where, n_t is the trap density, F_n is the electron fermi energy, k_B is the Boltzmann's constant and T_t is the characteristic temperature of the exponential trap distribution (i.e., T_t=E_t/k_B, where $E_t$is the characteristic trap energy). Solving Equations (1) and (2) with the above distribution of traps the current-voltage(J-V) characteristics has the form [21]:

$$J=N_C\mu^{(1-m)}\{\varepsilon m/H_n(m+1)\}^m\{(2m+1)/(m+1)\}^{(m+1)}V^{m+1}/L^{2m+1} \qquad (4)$$

Where m= T_t/T. The most notable feature in Equation (4) is the power-law dependence–V^{m+1}.

Fitting the experimental data for the dark I-V curve, as shown figure 2 and with the help of equation (4), we find that above the voltage 1.2 volt, the current voltage is fitted using the trap charge limited model and the value of m is equal to 0.53 and hence T_t is calculated to be159 K and E_t is calculated to be 0.013 eV.

3.1.2 Photocurrent measurement:

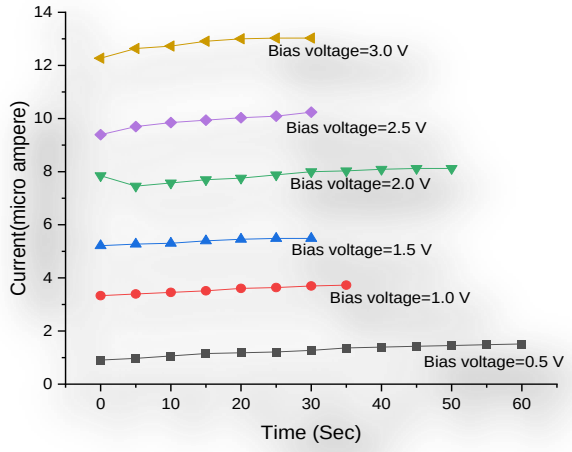

Fig- 3. Variation in photocurrent with time at different bias voltages

The photo current for this graphene oxide dye based solar cell (in photo-conducting mode) is measured with a Mastech MAS830L multimeter and photo current is plotted with time accordingly as shown in the figure 3 above. The photo current is found to be in micro ampere range. It is also found that the photo current increases with the increase in voltage. Theoretical analysis of| the photo-current data is not done here but a comparison of the value of photo current with and without graphene shows the enhanced effect as a result of incorporation of graphene in methyl orange dye based composite film.

3.2 Theoretical studies

In order to interpret the experimental findings, we choose model rGO system to develop nanocomposite with MO dye as shown in the figure 4 where rGO serves as an acceptor material and MO dye serves as a donor material. Ground state geometry optimization of the donor and acceptor nanocomposite revealed that rGO and MO dye is strongly interacted by shorter H bonds ranging from 2.22 Å to 2.80 Å yielding a high adsorption energy of -6.02 eV.

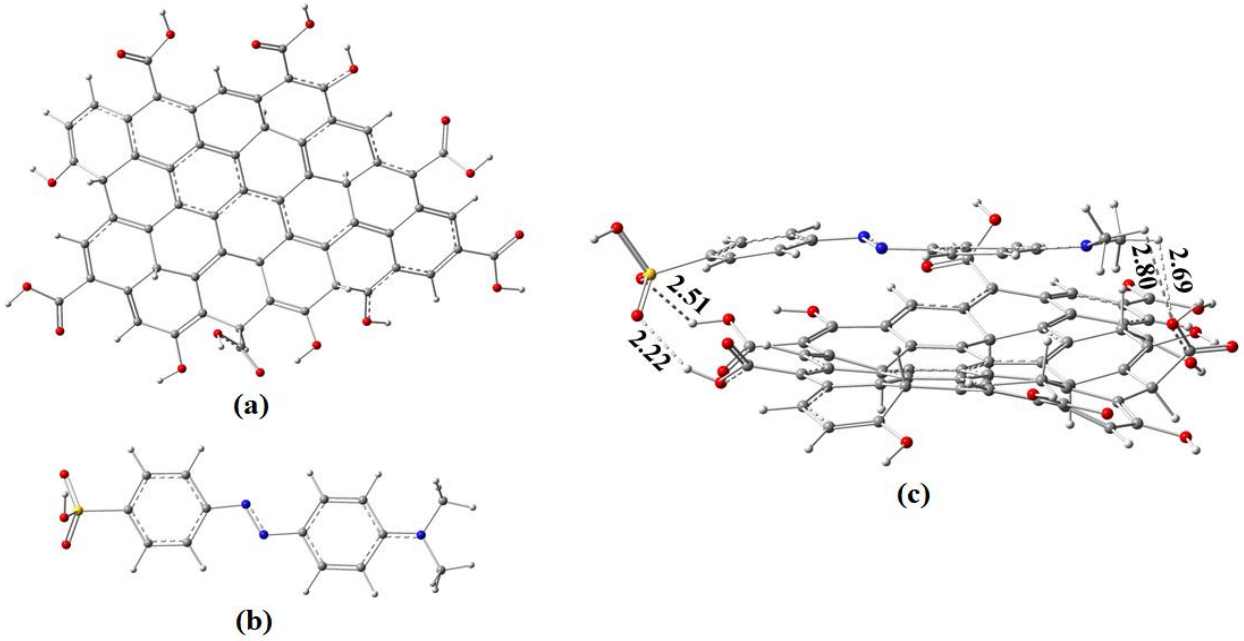

Fig-4. Ground state optimized structure of (a) Reduced Graphene Oxide (b) Methyl Orange (c) MO-rGO composite system Red, gray, white, and blue color represents oxygen, carbon, hydrogen, and nitrogen atoms respectively.

To analyze the excited state of the MO dye alongside the nanocomposite time dependent DFT(TD-DFT) were employed accounting all singlet excitation at the same level of theory. Excited state properties such as vertical excitation energies and oscillator strengths are computed from single point energy calculations of the excited state and tabulated in the Table 1a and 1b.

Table-1a Computed absorption wavelengths (λ_{max} in nm), vertical excitation energies (E_{0-0} in eV), oscillator strengths (f), the composition of the corresponding electronic transitions (H, HOMO; L, LUMO), calculated in water by using B3LYP/6–31 + G(d) level of theory MO dye.

States of Methyl Orange	λ_{max} (nm)	E_{0-0}(eV)	Oscillator Strength (f)	Major contributions
1	481.94	2.57	0.0868	H-1->LUMO (91%)
2	461.56	2.69	1.1511	HOMO `->LUMO (92%)
3	315.70	3.93	0.0135	H-3->LUMO (14%)
4	307.39	4.03	0.0015	H-4->LUMO (18%)
5	298.64	4.15	0.0913	H-4->LUMO (14%)
6	284.52	4.36	0.2159	H-4->LUMO (23%)
7	280.81	4.42	0.0029	H-4->LUMO (40%)
8	268.38	4.62	0.0281	H-3->LUMO (14%)
9	266.63	4.65	0.002	H-1->L+1 (92%)

10	254.81	4.87	0.0023	H-1->L+2 (96%)
11	251.82	4.92	0.0036	HOMO->L+4 (75%)
12	248.11	5.00	0.0146	HOMO->L+4 (23%)
13	238.46	5.20	0.0004	H-1->L+3 (96%)
14	237.60	5.22	0.0018	H-5->LUMO (87%)
15	225.80	5.49	0.0093	HOMO->L+6 (76%)
16	225.29	5.50	0.0012	HOMO->L+6 (13%)
17	216.65	5.72	0.053	H-4->L+1 (11%)
18	215.90	5.74	0.0254	HOMO->L+8 (83%)
19	215.49	5.75	0.0062	H-6->LUMO (88%)
20	213.70	5.80	0.0007	H-9->LUMO (41%)

Table-1b Computed absorption wavelengths (λ_{max} in nm), vertical excitation energies (E_{0-0} in eV), oscillator strengths (f), the composition of the corresponding electronic transitions (H, HOMO; L, LUMO), calculated in water by using B3LYP/6–31+G(d) level of theory nanocomposites.

States of composite system	λ_{max} **(nm)**	E_{0-0}**(eV)**	**Oscillator Strength (*f*)**	**Major contributions**
1	1724.64	0.72	0.0588	HOMO->LUMO (74%)
2	1339.07	0.93	0.0138	HOMO->L+1 (40%)
3	1196.41	1.04	0.0083	H-1->LUMO (76%)
4	1114.77	1.11	0.0787	HOMO->L+2 (34%)
5	1023.65	1.21	0.0883	H-2->LUMO (48%)
6	976.79	1.27	0.1155	HOMO->L+3 (64%)
7	846.66	1.46	0.004	H-1->L+2 (53%)
8	835.70	1.48	0.2979	H-1->L+1 (69%)
9	786.80	1.58	0.0118	H-2->L+1 (68%)
10	736.34	1.68	0.0095	H-2->L+2 (43%)
11	725.01	1.71	0.0665	HOMO->L+4 (32%)
12	711.29	1.74	0.0017	H-3->LUMO (98%)
13	695.13	1.78	0.0064	H-1->L+3 (87%)
14	663.94	1.87	0.135	H-4->LUMO (80%)
15	639.23	1.94	0.0001	H-2->L+3 (92%)
16	603.15	2.06	0.0655	HOMO->L+5 (57%)
17	593.74	2.09	0.0833	H-4->L+1 (50%)
18	591.36	2.10	0.002	H-3->L+1 (95%)
19	569.60	2.18	0.0339	H-3->L+2 (83%)
20	563.97	2.20	0.3144	H-1->L+4 (80%)

To comprehend the electron excitation process involving the reduced graphene oxide and methyl orange nanocomposite system energy band alignment some selected orbitals that determine the electron injection process of the dye viz. HOMO and LUMO energy levels of the individual components along with the electrodes are analyzed as shown in the figure 5.

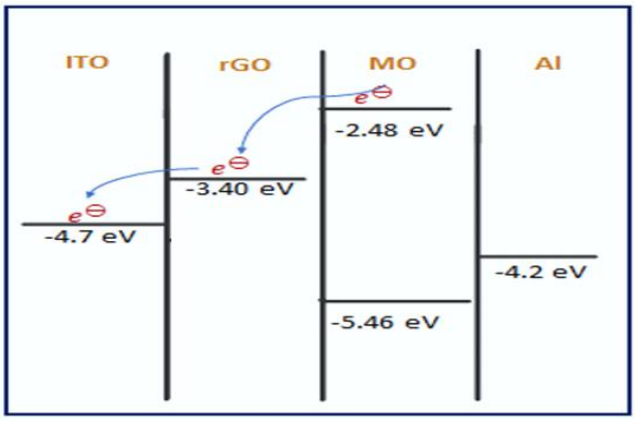

Fig- 5. Band alignment of rGO, MO dye in water

This scenario inevitably ensures the possibility of a photo-induced intramolecular charge transfer along the p-conjugated skeleton and finally electron injection from the dye to the conduction band of rGO.

With a view to gain insight into the light harvesting and optical properties of the MO dye, UV- spectra and corresponding absorption data are collected in table 1. From UV spectra analysis it is found that the absorption peak is at 461.56 nm which was contributed by HOMO-> LUMO transition. This value is concorded with the value of absorption peak of MO dye in aqueous solution which is found to be 463 nm [34]. Another peak occurs at 284.52 nm which was contributed by HOMO-4-> LUMO transition. The oscillator strengths corresponding to the peaks are 1.151 and 0.215 respectively. The oscillator strength is proportional to the intensity incident upon the dye. The amount of absorption increases with increasing value of oscillator strength. From the spectra it is evident that the dye (donor) absorbs light in the visible range and corresponding exited electrons are transferred to the rGO (acceptor). Hence the composite system can be used as a dye sensitized solar cell.

On analyzing the UV-spectra and corresponding absorption data of rGO-MO composite system, we found an absorption peak at 563.97 nm which extends over the infrared region ensuring the composite system is capable of harvesting the entire solar spectra as shown in figure 6. Compared to the peak of MO dye, the former is well inside the visible region. So, the rGO-MO composite system is a promising candidate for faithful photovoltaic applications.

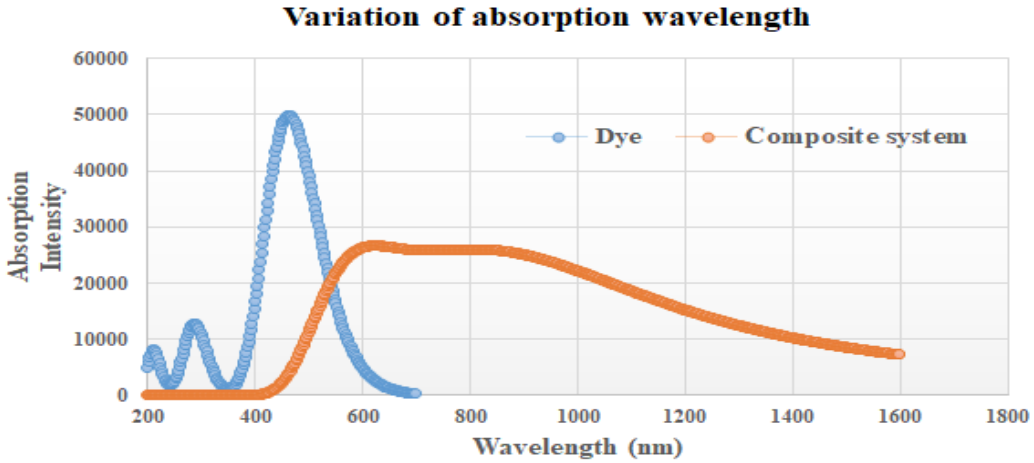

Fig- 6. Simulated UV-vis absorption spectra for MO dye and Composite system

We have even analyzed the electrostatic potential map of the composite system and found that enhanced electrostatic interaction between the rGO and MO exist (red region of the ESP map) as shown in the figure 7.

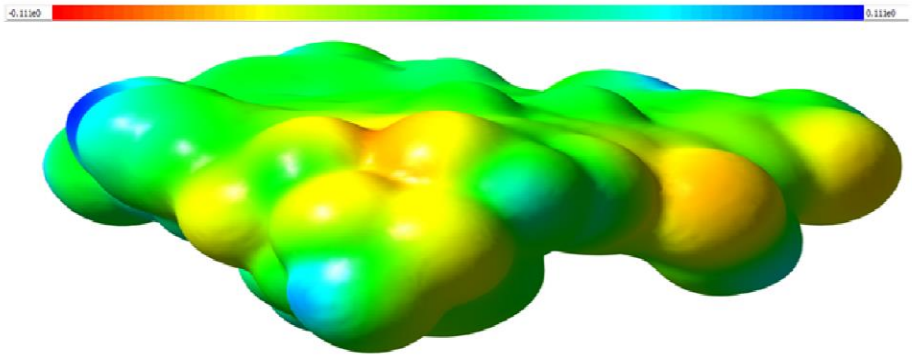

Fig- 7. Electrostatic potential map of rGO-MO composite system

To learn about the type of interactions between dye and clusters (Van der Waals interactions, steric interactions), non-covalent interaction (NCI) index plots of the reduced density gradient (RDG or s) vs. molecular density ρ were analyzed using the Multiwfn 3.7 suite. To identify the attractive and repulsive interactions, the eigenvalues (λi) of the second derivative of density are plotted within the framework of the non-covalent index technique. The stabilizing interactions are designated by negative values, while repulsive interactions are categorized by positive values of sign(λ2)ρ. NCI-RDG plots for MO-rGO composite system is shown in the figure 8

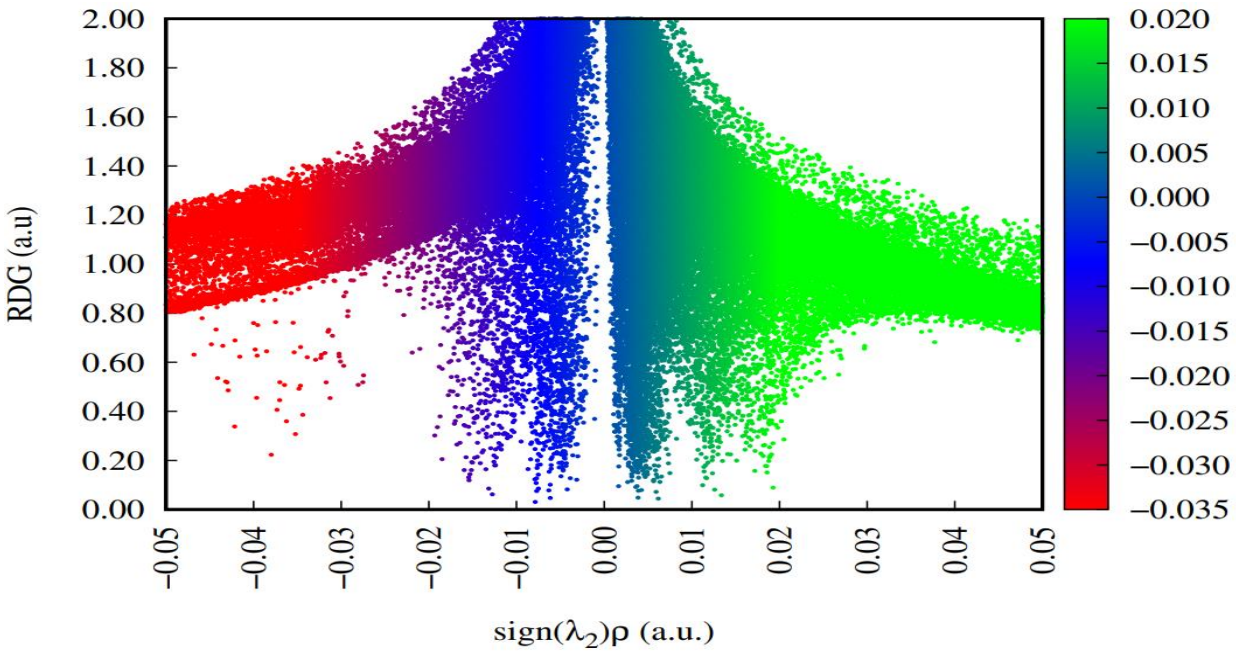

Fig- 8. RDG plots of MO-rGO composite system

In the plot, the blue region indicates Van der walls interactions while the red and green regions indicate strong attraction and steric repulsion respectively. It is clear from the plot that in the composite system taken, Van der walls interactions are prominent at the MO-rGO interface.

4. CONCLUSION

To summarize, graphene dye-based device has been designed and synthesized and was explored as non-fullerene acceptor nanomaterials. Fabrication of an organic solar cell by use of this stable acceptor was performed with in ambient atmosphere. Simulation of the device reveals that reduced graphene oxide and methyl orange makes a highly interacting nanocomposite system via shorter H bonding. Furthermore, DFT calculations also indicate the acceptable energy alignment and excellent acceptor capability for its| application in photovoltaic devices. TDDFT calculation reveal that when compared to MO dye the composite system is quite capable absorbing the whole radiation of the solar spectrum. It is evident form the energy alignment that this composite is suitable for flow of electron. Formation of nanocomposite formations via H bonding, appropriate alignment for electron transfer ensures a good device formation. Experimentally, the enhancement of photoconductivity as a result of incorporation of graphene in dye based PVA film were found. Study of the device's steady-state dark I-V characteristics explores the nature| of trap distribution because current conduction generally in most organic materials is controlled by trap distribution. Experimentally, we have found that above a threshold voltage of 1.2 volt, the conduction is organized by an exponential distribution of trap centres. Because the transition in our system is spread rather than abrupt, the trap levels are not concentrated in a single energy level. Within the experimental bounds, it has been estimated that one trap's temperature and energy level are, respectively, 159K and 0.013 eV. Studying the steady-state operation of a solar cell based on graphene dye nano composite will be made simpler with the use the experimental data.

Acknowledgement

We wish to acknowledge especially Prof. Kumaresh Ghosh, Department of Chemistry, University of Kalyani for supporting theoretical calculations.

References:

1. Gan, Q., Bartoli, F. J., &Kafafi, Z. H. (2013). Plasmonic-enhanced organic photovoltaics: Breaking the 10% efficiency barrier. *Advanced materials*, *25*(17), 2385-2396.

2. Pei, Q. (1996). Yang; Yu, G.; Zhang, C.; Heeger. J. Am. Chem. Soc, 118, 3922.

3. Green, M. A., Emery, K., Hishikawa, Y., & Warta, W. (2008). Solar Cell Efficiency Tables, Prog. Photovolt. *Res. Appl*, *16*, 61.

4. Bauhuis, G. J., Mulder, P., Haverkamp, E. J., Huijben, J. C. C. M., &Schermer, J. J. (2009). 26.1% thin-film GaAs solar cell using epitaxial lift-off. *Solar Energy Materials and Solar Cells*, *93*(9), 1488-1491.

5. Solar PV Manufacturing Cost Analysis. Available online: http://www.nrel.gov/analysis/key_activities_jobs_pv_mfg_cost.html (accessed on 10 October 2011).

6. Kumar, P., & Chand, S. (2012). Recent progress and future aspects of organic solar cells. *Progress in Photovoltaics: Research and applications*, *20*(4), 377-415.

7. Dou, L., You, J., Hong, Z., Xu, Z., Li, G., Street, R. A., & Yang, Y. (2013). 25th anniversary article: a decade of organic/polymeric photovoltaic research. *Advanced materials*, *25*(46), 6642-6671.

8. Zhou, N., Buchholz, D. B., Zhu, G., Yu, X., Lin, H., Facchetti, A., ... & Chang, R. P. (2014). Ultraflexible polymer solar cells using amorphous zinc− indium− tin oxide transparent electrodes. *Advanced Materials*, *26*(7), 1098-1104.

9. Tang, C. W. (1986). Two-layer organic photovoltaic cell. *Applied physics letters*, *48*(2), 183-185.

10. Rathore, N., Panwar, N. L., Yettou, F., & Gama, A. (2021). A comprehensive review of different types of solar photovoltaic cells and their applications. *International Journal of Ambient Energy*, *42*(10), 1200-1217.

11. Muchuweni, E., Martincigh, B. S., & Nyamori, V. O. (2020). Recent advances in graphene-based materials for dye-sensitized solar cell fabrication. *RSC advances*, *10*(72), 44453-44469.

12. Manzano-Ramírez, A., López-Naranjo, E. J., Soboyejo, W., Meas-Vong, Y., &Vilquin, B. (2015). A review on the efficiency of graphene-based BHJ organic solar cells. *Journal of Nanomaterials*, *2015*.

13. Xu, Y., Long, G., Huang, L., Huang, Y., Wan, X., Ma, Y., & Chen, Y. (2010). Polymer photovoltaic devices with transparent graphene electrodes produced by spin-casting. *Carbon*, *48*(11), 3308-3311.

14. Gao, X., Ma, W., Han, G., Chang, Y., Zhang, Y., & Li, H. (2019). The electrochemical properties of reduced graphene oxide film with capsular pores prepared by using oxalic acid as template. *International Journal of Energy Research*, *43*(14), 8177-8189

15. Jung, S., Lee, J., Choi, Y., Lee, S. M., Yang, C., & Park, H. (2017). Improved interface control for high-performance graphene-based organic solar cells. *2D Materials*, *4*(4), 045004.

16. Jung, S., Lee, J., Seo, J., Kim, U., Choi, Y., & Park, H. (2018). Development of annealing-free, solution-processable inverted organic solar cells with N-doped graphene electrodes using zinc oxide nanoparticles. *Nano letters*, *18*(2), 1337-1343.

17. Kim, H., Byun, J., Bae, S. H., Ahmed, T., Zhu, J. X., Kwon, S. J., ... & Lee, T. W. (2016). On-Fabrication Solid-State N-Doping of Graphene by an Electron-Transporting Metal Oxide Layer for Efficient Inverted Organic Solar Cells. *Advanced Energy Materials*, *6*(12), 1600172.

18. Jo, G., Na, S. I., Oh, S. H., Lee, S., Kim, T. S., Wang, G., ... & Lee, T. (2010). Tuning of a graphene-electrode work function to enhance the efficiency of organic bulk heterojunction photovoltaic cells with an inverted structure. *Applied Physics Letters*, *97*(21), 253.

19. Liu, Q., Liu, Z., Zhang, X., Zhang, N., Yang, L., Yin, S., & Chen, Y. (2008). Organic photovoltaic cells based on an acceptor of soluble graphene. *Applied Physics Letters*, *92*(22), 195.

20. Yu, D., Park, K., Durstock, M., & Dai, L. (2011). Fullerene-grafted graphene for efficient bulk heterojunction polymer photovoltaic devices. *The Journal of Physical Chemistry Letters*, *2*(10), 1113-1118

21. Farag, A. A. M., Mansour, A. M., Ammar, A. H., & Rafea, M. A. (2011). Characterization of electrical and optical absorption of organic based methyl orange for photovoltaic application. Synthetic Metals, 161(19-20), 2135-2143

22. M. SAMPIERTO, R. SOTGIU, F. P. WENZL, L. HOLZER, S. TASCH and G. LEISING, *ibid.* **61** (2000) 266

23. Burrows, P. E., Shen, Z., Bulovic, V., McCarty, D. M., Forrest, S. R., Cronin, J. A., & Thompson, M. E. (1996). Relationship between electroluminescence and current transport in organic heterojunction light-emitting devices. *Journal of Applied Physics*, *79*(10), 7991-8006

24. Yang, J., & Shen, J. (1999). Effects of discrete trap levels on organic light emitting diodes. *Journal of appliedphysics*, *85*(5),2699-2705.

25. Marcano, D. C., Kosynkin, D. V., Berlin, J. M., Sinitskii, A., Sun, Z., Slesarev, A., ... & Tour, J. M. (2010). Improved synthesis of graphene oxide. *ACS nano*, *4*(8), 4806-4814.

26. Zainuddin, M. F., Raikhan, N. N., Othman, N. H., & Abdullah, W. F. H. (2018, May). Synthesis of reduced Graphene Oxide (rGO) using different treatments of Graphene Oxide (GO). In *IOP Conference Series: Materials Science and Engineering* (Vol. 358, No. 1, p. 012046). IOP Publishing

27. Frisch, M.; Trucks, G.; Schlegel, H.; Scuseria, G.; Robb, M.; Cheeseman, J.; Scalmani, G.; Barone, V.; Petersson, G.; Nakatsuji, H., Gaussian 16. Gaussian, Inc. Wallingford, CT: 2016.

28. Cossi, M.; Barone, V.; Cammi, R.; Tomasi, J., Ab initio study of solvated molecules: a new implementation of the polarizable continuum model. *Chemical Physics Letters* **1996,** *255* (4-6), 327-335.

29. Lu, T.; Chen, F., Multiwfn: a multifunctional wavefunction analyzer. *Journal of computational chemistry* **2012,** *33* (5), 580-592.

30. Zhao, Y., & Truhlar, D. G. (2008). The M06 suite of density functionals for main group thermochemistry, thermochemical kinetics, noncovalent interactions, excited states, and transition elements: two new functionals and systematic testing of four M06-class functionals and 12 other functionals. *Theoretical chemistry accounts*, *120*, 215-241.

31. Miertuš, S., Scrocco, E., & Tomasi, J. (1981). Electrostatic interaction of a solute with a continuum. A direct utilizaion of AB initio molecular potentials for the prevision of solvent effects. *Chemical Physics*, *55*(1), 117-129.

32. O'boyle, N. M., Tenderholt, A. L., & Langner, K. M. (2008). Cclib: a library for package-independent computational chemistry algorithms. *Journal of computational chemistry*, *29*(5), 839-845.

33. Dey, S. K., Islam, M. R., Manik, N. B., & Basu, A. N. (2002). Study of the effect of trap levels on steady-state dark I–V characteristics in Safranine-T-based solid-state thin film photoelectrochemical cell. *Journal of Materials Science: Materials in Electronics*, *13*, 249-252.

34. Chen, Y. P., Liu, S. Y., Yu, H. Q., Yin, H., & Li, Q. R. (2008). Radiation-induced degradation of methyl orange in aqueous solutions. *Chemosphere*, *72*(4), 532-536.